European Journal of Physics

Debunking Boyle's self-flowing flask

European Journal of Physics

OPEN ACCESS

RECEIVED
26 September 2025

REVISED
21 November 2025

ACCEPTED FOR PUBLICATION
4 December 2025

PUBLISHED
31 December 2025

PAPER

Debunking Boyle's self-flowing flask

Daniele Battesimo Provenzano *

Classe di Scienze, Scuola Normale Superiore, Pisa, Italy

* Author to whom any correspondence should be addressed

E-mail: daniele.provenzano@sns.it

Keywords: Bernoulli's equation, perpetual motion, turbulence, viscous fluids, laminar flow, turbulent flow, unsteady Bernoulli's equation

Abstract

This paper investigates the widespread myth of perpetual motion devices based on the so-called Boyle's self-flowing flask, frequently popularized in online videos. A simplified theoretical model is developed to describe the dynamics of the system, showing that the flow inevitably decays and that the maximum operating time is only a few seconds for realistic geometries. Simple original tabletop experiments with hoses of different sizes confirm this picture, yielding even shorter operating times due to the additional dissipation caused by turbulence. It is of course trivial to remark that perpetual motion is impossible; what is perhaps less obvious, and what our analysis demonstrates, is that the fountain mechanism itself cannot last more than a few seconds in practice, thereby debunking the fake videos circulating on the internet. The theoretical analysis developed in this paper can serve as a useful introduction to the generalization of Bernoulli's equation to viscous and unsteady flows, making it suitable for inclusion in a graduate-level fluid dynamics course. On the other hand, the experimental side is accessible to anyone, requiring only simple materials and thus offering an engaging way to illustrate fundamental fluid dynamics concepts.

1. Introduction

The concept of perpetual motion has fascinated humankind for millennia, even though it is well known that such a phenomenon cannot occur because of the inevitable dissipative effects that characterize the physical world [1–3]. Despite this, the internet has recently become increasingly filled with click-bait videos claiming to demonstrate perpetual motion, typically involving water circulating through small ducts or balls rolling endlessly along tracks, as discussed, for instance, in [4]. Among these configurations, the most popular example is the one illustrated in figure 1, known as Boyle's self-flowing flask, which consists of a water container that supposedly refills itself continuously through a uniform cross section hose. In these videos—often titled 'Perpetual Motion Machine' or similar—the flow appears to be never-ending and perfectly steady [5]. Needless to say, these videos are fabricated: the system inevitably loses mechanical energy for various reasons, including viscous effects, turbulence [6, 7], and collisions with the container walls, so this motion cannot persist indefinitely. Even the sound of water falling back into the container is clear evidence of this loss.

There are also almost-correct educational videos that aim to debunk these claims, but they often introduce their own inaccuracies [8]. A common misconception in fluid dynamics, for example, is that energy losses are purely due to viscosity. Many believe that using a superfluid—characterized by zero viscosity—would enable a true perpetual motion device. Even setting aside the quantum effects associated with superfluidity, this is very unlikely to be the case. From a purely theoretical standpoint, a recently resolved conjecture, originally proposed by Onsager in [9], states that above a certain degree of turbulence—namely, when the velocity field becomes sufficiently irregular—energy is dissipated even though $\mu = 0$, through the mechanism known as anomalous

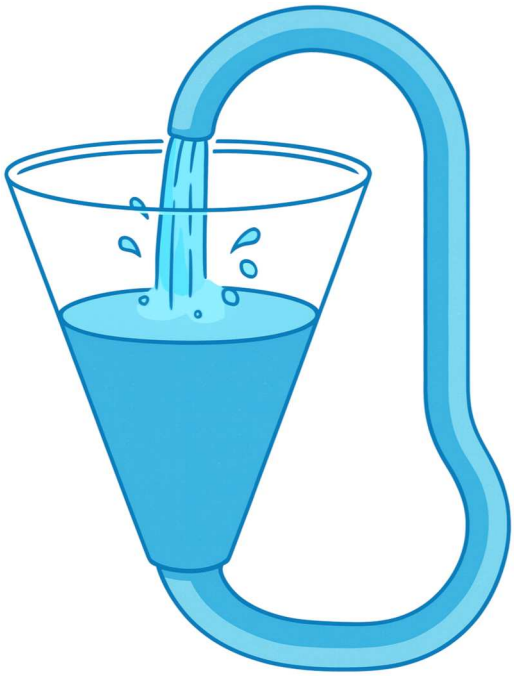

Figure 1. Schematic illustration of the setup used to generate the fake perpetual motion.

dissipation. It is not useful to reproduce the precise mathematical statement here; interested readers are referred to [10, 11]. In short, perpetual motion cannot exist even in ideal fluid dynamics.[1]

To this day, the fascination of turbulence and our limited understanding of it place the phenomenon at the forefront of research in mathematical physics. It suffices to recall that the Navier–Stokes equations are the subject of one of the Millennium Prize Problems [12]. In the case illustrated in figure 1, turbulence is inevitably generated in the region where the water jet falls and mixes with the nearly still water in the container. As we shall see later, this is an effect that cannot be neglected and that prevents the application of Bernoulli's equation—even in its most general form—because it corresponds to a flow that is intrinsically and unpredictably unsteady and rotational. Therefore, we will apply Bernoulli's equation only in regions where the flow can reasonably be considered laminar and ordered.

Although earlier pedagogical discussions have been largely qualitative [2–4, 13], the present work offers a quantitative theoretical analysis of a simplified version of the configuration shown in figure 1. We demonstrate that, for realistic parameters, the operating time of the device does not exceed a few seconds, thus conclusively debunking these myths. More specifically, we perform the theoretical calculations under the assumption that no turbulence occurs inside the hose,[2] thus obtaining an upper bound for the operating time. Experimental tests yield even shorter operating times because the flow within the hose is actually turbulent, since Reynolds number exceeds $\mathrm{Re} \sim 4000$. In this sense, the theoretical predictions should be interpreted as an upper bound corresponding to the least dissipative case. The difference between the two regimes, as discussed later, also provides an instructive example of how viscosity and turbulence influence real flows and of how a more viscous fluid, such as oil, would make the theoretical and experimental results converge.

The paper is organized as follows:

[1] On the experimental side, only limited evidence of anomalous dissipation has been reported, since research in this area is still underdeveloped: no dedicated experiments have yet been carried out. A naive argument usually invoked is that the drag coefficient of a body moving in a fluid tends to a nonzero value for very large Reynolds numbers, but this is still far from proving that reality fully matches the mathematical model. Due to the delicacy of the subject and the high potential for error, the limit $\mu \to 0$ will only be briefly mentioned in this work, without further elaboration. For a broader and more detailed overview of the topic, we refer the reader to [11].

[2] The assumption of laminar flow within the hose is adopted primarily for analytical tractability: it allows the governing equations to be solved in closed form without resorting to empirical friction factors or semi-empirical turbulence models. A fully quantitative description of the turbulent regime would require Reynolds-number-dependent Darcy–Weisbach coefficients, roughness parameters, and other empirical correlations [14], leading to an evolution equation that must be integrated numerically. Incorporating these ingredients would considerably complicate the analysis while adding several empirical parameters, thereby weakening its pedagogical clarity. By contrast, the laminar formulation isolates the essential physical mechanisms—viscosity and unsteadiness—within a transparent analytical framework, and at the same time provides a rigorous upper bound for the operating time, since any realistic turbulent model would only increase the overall dissipation.

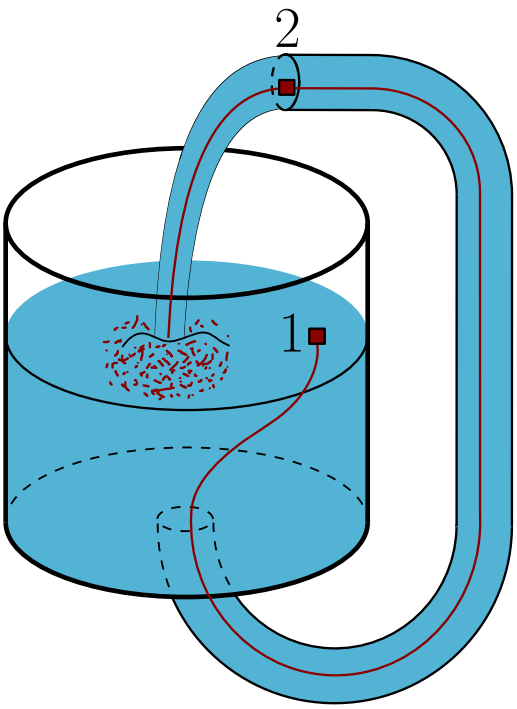

Figure 2. Schematic illustration of the streamline considered in equation (4). The jagged red segment indicates where the streamline breaks due to turbulence.

1. Section 2 presents the theoretical model, based on the unsteady and viscous generalization of Bernoulli's equation, under the assumptions of incompressible fluid and laminar flow within the hose. Some energetic considerations are also introduced, formally showing that the mechanical energy of the system decreases over time. The theoretical framework adopted here is significantly more general than those used in classical draining or filling problems, which usually extend Bernoulli's equation either to the unsteady case or to the viscous case [15–17], but not both simultaneously. In this work, by contrast, we consider the two effects at once. Moreover, by separating laminar and turbulent regions, the analysis makes explicit where and why Bernoulli's equation applies (or may fail), which students often find conceptually elusive.
2. Section 3 compares the theoretical upper bound for the operating time with experiments that can be easily performed at home using a bucket and a garden hose. These experiments were specifically designed and carried out for this study and are based on separating two sections of the same hose.

To avoid confusion in terminology, throughout this paper the word 'hose' will refer exclusively to the curved tube shown in figure 2, while the term 'ducts' will denote the entire assembly consisting of the container and the hose, which together form axially symmetric conduits.

2. Theoretical model

We begin by making our initial assumptions explicit. We shall assume that water behaves as an incompressible fluid and that the only form of turbulence present is that generated when the water jet falls back into the container. Other forms of turbulence, such as that which may arise when the cross section of the ducts narrows abruptly, are not straightforward to treat and would require models based on empirical coefficients. Therefore, with reference to figure 2, we assume that the junction in the hole, between the bottom of the container and the end of the hose, is round-shaped, thus eliminating the vena contracta effect and the associated head loss [18–21]. From the experimental standpoint, this assumption is justified by the use of grommets at the inlet, as will be described in section 3. Finally, we assume that the Reynolds number associated with the flow in the hose is sufficiently low for the flow to remain laminar in that region.

The goal of this analysis is to determine how long the flow in figure 2 will last, assuming we manage to impart an initial velocity[3] v_0 to the water inside the hose—for instance, by initially draining the container with

[3] Since viscous effects are taken into account, the velocity varies over the cross section. Throughout this work, whenever a velocity is mentioned, it is understood as the cross-sectional average of the velocity profile.

the hose held vertically, and then quickly moving its outlet end into the position shown in the figure, as done in many of the aforementioned videos.

Let S_C be the cross section of the container, S the cross section of the hose, L its length, $v_p(t)$ the velocity of water in the hose, h the height of the water surface in the container, and H the height of the upper end of the hose, both measured from the bottom of the container. Because water can be treated as an incompressible fluid, the conservation of the volumetric flow rate implies that h remains constant over time. This does not mean that the water surface velocity is zero. In fact, neglecting the turbulent region where the velocity field is irregular, conservation of mass gives

$$S\, v_2 = S_C\, v_1, \tag{1}$$

where the velocities refer to the corresponding points shown in figure 2.

2.1. Unsteady viscous Bernoulli's equation

Since we want to study the time evolution of the system in figure 2, using only the steady version of the governing equations is insufficient. In particular, since h and H are constant, the restricted Bernoulli's equation,

$$p(\vec{r}) + \frac{1}{2}\rho v^2(\vec{r}) + \rho g z = \text{const.}, \tag{2}$$

namely, the form of Bernoulli's equation that relies on the strongest set of assumptions, would predict the same velocity at all times while neglecting viscosity altogether. However, our aim is to show that the velocity decreases over time as a result of the dissipation of energy. The most general and appropriate tool for this is the unsteady viscous Bernoulli's equation [22, 23]:

$$p(\vec{r}) + \frac{1}{2}\rho v^2(\vec{r}) + \rho g z + \frac{8\mu Q}{\pi}\int_{s_0}^{s}\frac{\mathrm{d}s'}{r^4(s')} + \rho\int_{\vec{s}_0}^{\vec{s}}\frac{\partial\vec{v}}{\partial t}\cdot\vec{\mathrm{d}s'} = \text{const.}, \tag{3}$$

which holds for unsteady laminar flows of incompressible, viscous fluids in axially symmetric conduits (i.e. ducts with rotational symmetry about their axis). Here, Q is the volumetric flow rate, uniform throughout the ducts since the fluid is incompressible, s is the curvilinear coordinate along a generic streamline, s_0 denotes a reference point on the streamline, and $r(s)$ is the local cross-sectional radius of the duct at position s. As already mentioned, part of the flow is affected by turbulence, which invalidates the laminar assumption required to use equation (3). However, we will apply this equation only in regions where the flow is laminar and the streamlines are smooth, staying well away from the turbulent zones.

For simplicity, we could analyze equation (3) in the limit where the cross section of the container is much larger than that of the hose. However, we will treat the general case, so that notable limiting cases can be checked explicitly later. Equation (3), applied along the streamline passing through points 1 and 2 in figure 2,[4] reads

$$p_{\text{atm}} + \frac{1}{2}\rho v_1^2 + \rho g h = p_{\text{atm}} + \frac{1}{2}\rho v_2^2 + \rho g H + \frac{8\pi\mu}{S}\left[\left(\frac{S}{S_C}\right)^2 h + L\right]v_p + \rho\int_{\vec{s}_1}^{\vec{s}_2}\frac{\partial\vec{v}}{\partial t}\cdot\vec{\mathrm{d}s}. \tag{4}$$

Here we have assumed that the streamline is approximately vertical inside the container, as done in [15–17]. Strictly speaking, this assumption is valid, provided that $h \gg \sqrt{S_C}$, except in the region very close to the bottom. Equation (4) is essentially Newton's second law applied to the flow, where the last term represents acceleration.

Except for the region in the container close to the hole, the velocity field at a fixed t is piecewise constant:

$$\vec{v}(\vec{s},\, t) \approx \begin{cases} \frac{S}{S_C}\, v_p(t)\,\hat{s} & \text{if} \quad \vec{s} \in \text{container}, \\ v_p(t)\,\hat{s} & \text{if} \quad \vec{s} \in \text{hose}. \end{cases} \tag{5}$$

Thus, the unsteady term becomes

$$\int_{\vec{s}_1}^{\vec{s}_2}\frac{\partial\vec{v}}{\partial t}\cdot\vec{\mathrm{d}s} \approx \left(\frac{S}{S_C}\,h + L\right)\frac{\mathrm{d}v_p}{\mathrm{d}t}. \tag{6}$$

Recalling that $v_2 = v_p$ and simplifying, equation (4) reduces to

$$\rho\left(\frac{S}{S_C}\,h + L\right)\frac{\mathrm{d}v_p}{\mathrm{d}t} = \frac{1}{2}\rho v_p^2\left[\left(\frac{S}{S_C}\right)^2 - 1\right] - \frac{8\pi\mu}{S}\left[\left(\frac{S}{S_C}\right)^2 h + L\right]v_p + \rho g\,(h - H), \tag{7}$$

[4] Point 1 must be chosen sufficiently far from the turbulent region where the jet impacts the water in the container, so that it actually lies on a smooth streamline.

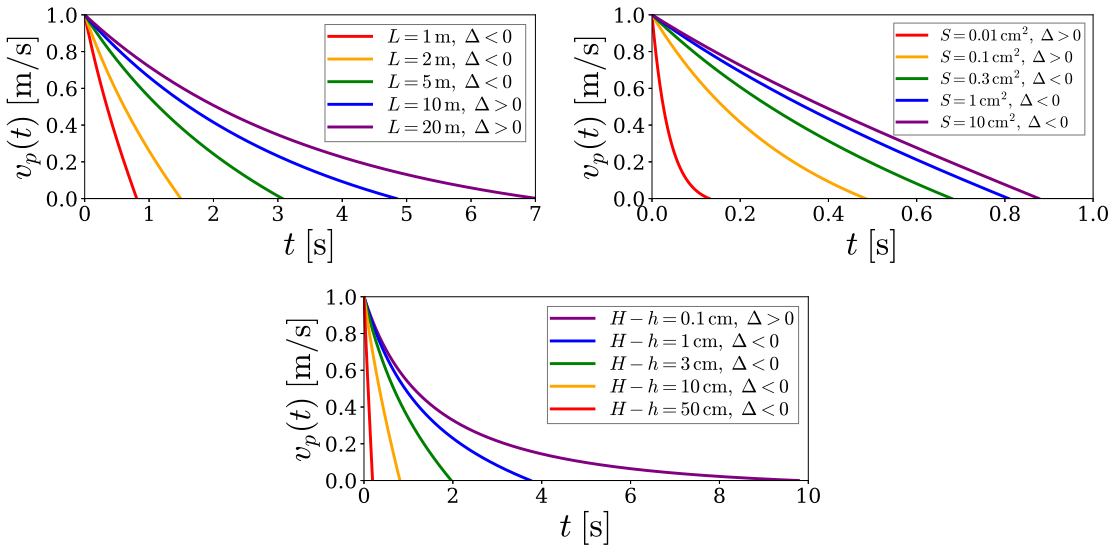

Figure 3. Flow velocity inside the hose as a function of time, for different values of the hose length L, the cross-sectional area S, and the height difference $H - h$.

to be solved with the initial condition $v_p(0) = v_0$. The solution is valid only within the time domain $[0, t_f]$, where t_f denotes the first instant when the velocity vanishes, i.e. $v_p(t_f) = 0$. Once the velocity drops to zero, it remains zero forever. Otherwise, energy would be generated out of nothing.

By defining the constant quantities

$$W \equiv \frac{S}{S_C} h + L > 0, \quad X \equiv \frac{1}{2}\left[\left(\frac{S}{S_C}\right)^2 - 1\right] < 0,$$
$$Y \equiv -\frac{8\pi\mu}{\rho S}\left[\left(\frac{S}{S_C}\right)^2 h + L\right] < 0, \quad Z \equiv g(h - H) < 0, \tag{8}$$

the Cauchy problem becomes

$$W \frac{\mathrm{d}v_p}{\mathrm{d}t} = X\, v_p^2 + Y\, v_p + Z, \qquad v_p(0) = v_0. \tag{9}$$

Introducing

$$\Delta \equiv Y^2 - 4XZ, \tag{10}$$

we can distinguish three different scenarios for the solutions, which differ according to the sign of Δ. Fortunately, exact analytical expressions for the solutions can be derived, as discussed in the Appendix.

Figure 3 shows the time evolution of the solution of equation (9) as the parameters L, S and $H - h$ vary. The values of the parameters common to all the graphs are $v_0 = 1\ \mathrm{m\ s^{-1}}$, $\rho = 10^3\ \mathrm{kg\ m^{-3}}$, $\mu = 10^{-3}$ Pa s, and the assumption $S_C \gg S$ is always satisfied.

It can be observed that the operating time increases with L and S, since both contribute to the total momentum inside the hose, while it decreases with $H - h$, as, given the form of Z in equation (8), increasing this quantity is equivalent to increasing the gravitational acceleration. This latter dependence will be analyzed and experimentally verified in section 3. Naturally, while keeping all other parameters fixed, the operating time is an increasing function of v_0 and a decreasing function of μ.

We now examine two noteworthy limiting cases.

1. Hose closed onto itself, forming a generic smooth closed curve Γ, as shown in figure 4. In this case, $S_C = S$ and $h = H$, so in equation (9) the coefficient of the term of highest degree vanishes. The equation must therefore be solved again from scratch to avoid singularities. Since $X = Z = 0$, the differential equation becomes

$$\frac{\mathrm{d}v_p}{\mathrm{d}t} = -\frac{8\pi\mu}{\rho S}\, v_p, \tag{11}$$

which is nothing but Newton's second law for a body slowed down by a drag force. As expected, since the flow forms a closed loop, gravity has no effect: the evolution of the system does not depend on the spatial

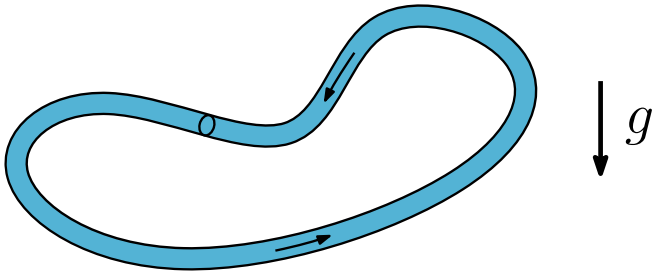

Figure 4. Water hose closed onto itself.

orientation of the hose, which could even lie on the ground, nor on the curve Γ that describes its path. The solution of equation (11) is an exponentially decaying function, so the operating time is formally infinite, even though the system continuously loses energy. If, moreover, $\mu = 0$, it might appear that a perfectly steady perpetual motion ($\dot{v}_p = 0$) could be achieved. However, in this limit the Reynolds number diverges, the flow becomes fully turbulent, and Bernoulli's equation can no longer be applied. Instead, the considerations outlined in section 1 on anomalous dissipation come into play.

2. *Absence of gravity*. If gravity is switched off—for instance, by performing the experiment in free fall or on the ISS—and provided that the surrounding air pressure is not so low as to trigger cavitation, one has $Z = 0$, which corresponds to the case $\Delta > 0$. In this situation, $v_- = 0$, and therefore equation (20) yields an infinite operating time, because the velocity decreases monotonically in time as an exponential function. This behavior is analogous to that shown in figure 3(c), since, by definition of Z, reducing g is equivalent to reducing $|H - h|$.

2.2. Energy considerations

We now focus on examining the temporal evolution of the system from an energetic perspective. Given the presence of dissipation, we expect the total mechanical energy of the system to decrease over time. Since the potential energy remains constant, the correct energy balance equation should return a total variation of energy equal to the initial kinetic energy associated with the motion.

The energy lost to viscous effects associated with the laminar flow in the ducts is[5]

$$\int_0^{t_f} 8\pi\mu \left[h\left(\frac{S}{S_C}\right)^2 v_p^2 + L v_p^2 \right] \mathrm{d}t, \tag{12}$$

while the energy lost in the turbulent region, i.e. where the jet touches the water in the container, is[6]

$$\int_0^{t_f} \left[\frac{1}{2}\rho S \left[1 - \left(\frac{S}{S_C}\right)^2 \right] v_p^3 + \rho g (H - h) S v_p \right] \mathrm{d}t. \tag{13}$$

Summing equation (12), (13) gives

$$\Delta E_{VT} = S \int_0^{t_f} \left\{ \frac{1}{2}\rho \left[1 - \left(\frac{S}{S_C}\right)^2 \right] v_p^2 + \rho g (H - h) + \frac{8\pi\mu}{S} \left[h\left(\frac{S}{S_C}\right)^2 v_p + L v_p \right] \right\} v_p \, \mathrm{d}t. \tag{14}$$

[5] Equation (12) represents the time integral of the power dissipated in the ducts. In a single pipe of length l, such power is $P = 8\pi\mu l v^2$, where v is, as usual, the average velocity over the cross section. This result can be easily found in [24, 25].

[6] In regions where the streamlines break and intertwine continuously, turbulence and viscous effects dissipate all the kinetic energy of the fluid. Hence, the dissipated power is generally given by $\frac{1}{2}\rho v^2 \times Q$, i.e. the product of the kinetic energy density and the volumetric flow rate. The conservation of mechanical energy associated with the free-fall motion yields

$$\frac{1}{2}\rho v^2 \times Q = \left(\frac{1}{2}\rho v_p^2 + \rho g (H - h) \right) \times S \, v_p,$$

which is still not exactly equal to equation (13). The reason is that one must also account for the relative motion of the jet with respect to the water moving downward in the container. For instance, if they both moved with the same velocity and in the same direction, there would be no collisions between the two flows, and thus no energy would be dissipated. This explains the presence of the additional term $-\frac{1}{2}\rho S v_1^2 \times Q = -\frac{1}{2}\rho S \left(\frac{S}{S_C}\right)^2 v_p^3$ in equation (13), accounting for the motion of the water level within the container.

By substituting the quantities inside the curly brackets using equation (7), we obtain

$$\begin{aligned}\Delta E_{\mathrm{VT}} &= -S\int_0^{t_{\mathrm{f}}}\left\{\rho\left(\frac{S}{S_{\mathrm{C}}}\,h+L\right)\frac{\mathrm{d}v_p}{\mathrm{d}t}\right\}v_p\,\mathrm{d}t\\ &= \frac{1}{2}\rho S\left(\frac{S}{S_{\mathrm{C}}}\,h+L\right)\Big[\,v_p^2\,\Big]_{t_{\mathrm{f}}}^{0}\\ &= \frac{1}{2}\rho S\left(\frac{S}{S_{\mathrm{C}}}\,h+L\right)v_0^2,\end{aligned}\tag{15}$$

which, apart from the turbulent contributions, is the initial kinetic energy of the entire fluid, since in general

$$\begin{aligned}K &= \sum_i(\text{kinetic energy density})_i\times(\text{volume})_i\\ &= \frac{1}{2}\rho\sum_i v_i^2\times V_i\\ &= \frac{1}{2}\rho v_p^2\,(SL)+\frac{1}{2}\rho\left(\frac{S}{S_{\mathrm{C}}}\right)^2 v_p^2\,(S_{\mathrm{C}}\,h).\end{aligned}\tag{16}$$

Thus, the energy balance yields exactly the result anticipated from the outset.[7]

3. Experiments

In this section, rather than providing an experimental test that validates the theoretical model, we offer a qualitative demonstration. As already anticipated in section 1, the Reynolds number associated with the water flow in the ducts exceeds the threshold that guarantees the assumption of laminar flow. Indeed,

$$\mathrm{Re}\approx\frac{2r\,v\,\rho}{\mu}\;\approx\;(2\;\times\;10^6\ \mathrm{m^2\,s^{-1}})\,r\,v,\tag{17}$$

where r is the local radius of the duct and v is the mean velocity of water at that location. Let us consider the most favorable case: using a tube with an internal radius of 3 mm and letting the water flow at an initial velocity on the order of 1 m s^{-1}. Since the viscosity of water is $\mu\approx10^{-3}$ Pa·s, this would give Re $\approx$ 6000, well above the threshold of 2300–4000 generally associated with the transition from laminar to turbulent flow in cylindrical pipes [14, 26]. Consequently, the flow is turbulent even inside the hose, which means that the theoretical predictions made in section 2 do not hold exactly but instead provide an upper bound for the operating time of the fountain. In fact, the presence of turbulence enhances energy dissipation, thereby reducing t_{f}.

One might think that it would suffice to reduce r or v, or increase μ, to enforce Re $<$ 2300. However, none of these approaches are viable. Using tubes with significantly smaller radii is unfeasible due to the onset of capillary effects and the drastic reduction of t_{f}. The same reasoning applies to imparting much smaller initial velocities (e.g. well below 1 m s^{-1}) or to using a more viscous liquid such as oil: in both cases, the operating time would become too short to be appreciable. One would need access to an actual oil reservoir in order to remain in the laminar regime while still maintaining a high initial velocity.

It is important to clarify that the upper bound introduced in section 2.1 should not be interpreted as a quantitative prediction for the experimental operating time, but rather as the least dissipative scenario compatible with the same geometry and initial conditions. In the theoretical model, wall friction inside the hose is treated as laminar, which minimizes the total energy losses. Any additional source of dissipation—such as turbulence, minor losses at the inlet and outlet, or bending—can only accelerate the decay of motion. The theoretical curve therefore represents the slowest admissible evolution of the flow and an upper limit for the operating time t_{f}.

For the experimental measurements, the main challenge was how to impose the initial velocity v_0 inside the pipe and how to set the spatial arrangement sketched in figure 2. At first, we attempted to achieve this by quickly lifting the pipe after letting the water start flowing, in the same way as shown in the videos cited in section 1. Unfortunately, this method is unsuitable for a quantitative analysis: it is unclear when to start measuring time and, moreover, by lifting the hose upward, one effectively increases (non-uniformly) the value of g, which, as explained earlier, shortens the operating time. After several failed attempts, we came up with the siphon configuration illustrated in figure 5.[8] The procedure works as follows:

[7] The same conclusion also holds in the case $\mu=0$: energy is dissipated solely within the (much larger) turbulent region through the mechanism discussed in section 1, until the flow eventually comes to an end.

[8] To our knowledge, this method has not been previously reported. We believe that it contains some original features, especially the one described in point 2, and we are pleased to present it here in the hope that it may serve as a useful tool for future experiments and demonstrations.

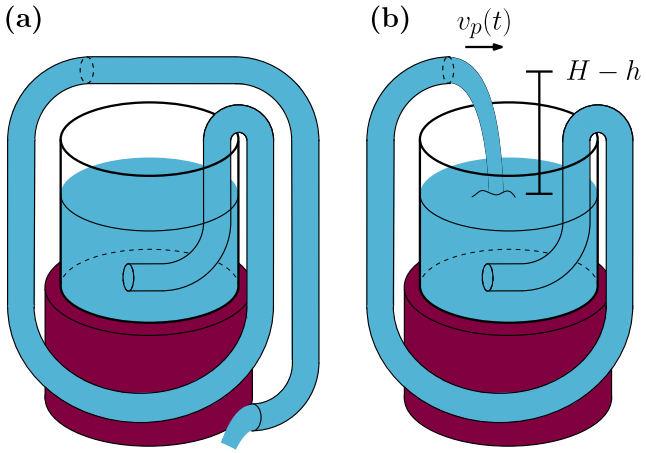

Figure 5. Schematic of the original configuration used for the experimental measurements. Once the flow reaches steady state [case (a)], the two tubes are disconnected so that water begins to flow out from the upper end of the tube partially immersed in the container [case (b)].

1. First, we operate the siphon mechanism shown in figure 5(a), consisting of two hoses of equal cross section joined with duct tape, while the container is continuously overfilled from a water source and allowed to overflow, thus keeping the water level constant. The initial flow velocity v_0 is then measured through a simple emptying experiment: knowing that the volume of water emptied in a generic time interval Δt is $V = v_0 S \Delta t$, measuring V and Δt allows us to determine v_0.[9]
2. Next, while the water flows through the hose, the two pipes are pulled apart by applying some force with the hands, allowing for the measurement of the operating time t_f of the jet shown in figure 5(b).

Because the experimental values of t_f are rather small, they were measured from the trials video using the software Tracker [27]. Particular care was taken to avoid excessive bending of the hose and to maintain a smooth curvature, in order to minimize additional losses. Another practical refinement was to insert a grommet, with the same internal radius as the hose, at the end of the submerged tube: as shown in [28], grommets mitigate the vena contracta effect by gradually reducing the cross section of the ducts. In particular, the authors show that the discharge coefficient—defined as the ratio between the actual mass flow rate and the theoretical mass flow rate—can increase from about 0.65 to nearly 1 by using simple industrial grommets.

The above routine was repeated for two different types of hoses (a standard garden hose with an inner radius of 7 mm, and a narrower hose of 3 mm) and for various values of their lengths and $H - h$. Note that in this case, the value of L obviously refers only to the single hose in figure 5(b), not to the union of the two hoses in figure 5(a). Data for all analyzed configurations are reported in table 1. The values of $H - h$ were set using a partially submerged vertically oriented ruler. Measurements were performed at an ambient temperature of approximately 26 °C, with the water temperature around 20 °C, letting $\mu = 10^{-3}$ Pa·s [29].

As can be seen in the table, the experimental times are consistently shorter than those predicted by theory. As already anticipated, this is due to turbulence in the water flow within the hose, which accelerates the dissipation of kinetic energy and shortens t_f.

For completeness, we briefly comment on the main sources of experimental uncertainty. The timing of the operating time t_f is affected by the frame rate and manual frame selection in the Tracker software, as well as by the finite response time of the observer. Despite our efforts to keep the hose curvature smooth, small residual bending cannot be completely excluded, and may introduce additional minor head losses. Furthermore, slight fluctuations of the water level in the container and of the height difference $H - h$ are unavoidable during each run. These effects vary randomly from one trial to the next and therefore manifest themselves as run-to-run fluctuations in the measured operating time. Their combined influence appears experimentally as scatter in the repeated measurements, which we quantify through the sample standard deviation reported in table 1.
Figure 6(a) shows the experimental times for the six configurations analyzed, plotted as a function of $H - h$, together with error bars corresponding to the sample standard deviation. Instead, figure 6(b) reports the percentage difference between the experimental times and those predicted by the theoretical model, evaluated

[9] As one might expect, v_0 cannot be computed *a priori* by applying formulas to the siphon, since the Reynolds number would be infinite inside the hose. The only reliable way to determine is by performing experiments.

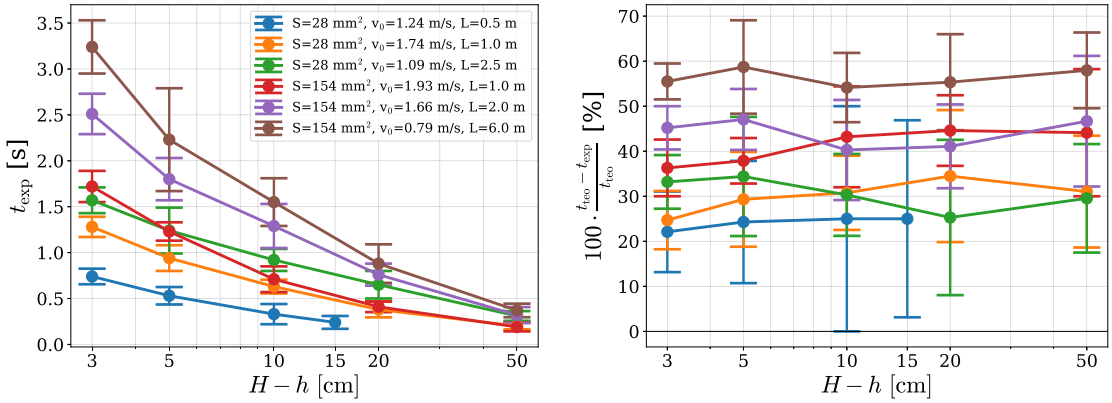

Figure 6. Comparison between experimental times (left) and percentage deviation from the theoretical model (right). The horizontal axis is shown on a logarithmic scale in both figures.

Table 1. Data collected from the experiments. Each value in the experimental time column is the average of five measurements; the uncertainty is the sample standard deviation over those five trials.

S (mm^2)	L (m)	v_0 ($m\ s^{-1}$)	$H-h$ (cm)	Exp. time (s)	Theo. time (s)
28	0.5	1.24	3.0	0.74(9)	0.95
			5.0	0.53(10)	0.70
			10.0	0.33(11)	0.44
			15.0	0.24(7)	0.32
	1.0	1.74	3.0	1.28(11)	1.70
			5.0	0.94(14)	1.33
			10.0	0.63(8)	0.91
			20.0	0.37(9)	0.58
			50.0	0.20(4)	0.29
	2.5	1.09	3.0	1.57(14)	2.35
			5.0	1.24(25)	1.89
			10.0	0.92(12)	1.32
			20.0	0.65(15)	0.87
			50.0	0.31(5)	0.44
154	1.0	1.93	3.0	1.72(17)	2.70
			5.0	1.23(10)	1.98
			10.0	0.71(14)	1.25
			20.0	0.41(6)	0.74
			50.0	0.19(5)	0.34
	2.0	1.66	3.0	2.51(21)	4.58
			5.0	1.80(23)	3.40
			10.0	1.29(24)	2.16
			20.0	0.76(12)	1.29
			50.0	0.32(9)	0.60
	6.0	0.79	3.0	3.24(29)	7.28
			5.0	2.23(56)	5.40
			10.0	1.55(26)	3.38
			20.0	0.88(21)	1.97
			50.0	0.37(7)	0.88

using equation (9), corresponding to each point in figure 6(a). Notice that the percentage differences for the 7 mm hose are clearly greater than those for the 3 mm hose. This can be explained by the fact that the Reynolds number associated with the larger hose is about twice that of the smaller one. As a result, turbulence effects are even stronger in the larger hose, leading to faster dissipation, and consequently to a greater percentage difference in operating time.

It is also worth noting that the theoretical model would become quantitatively more accurate for a more viscous liquid. If the same setup were repeated using oil instead of water, the Reynolds number would drop well below the transition threshold, leading to a fully laminar flow inside the hose. In that case, the experimental data would approach much more closely the theoretical upper bound. From a didactic perspective, this observation is particularly valuable: it shows how the same physical principles apply across regimes, and how the comparison between different fluids can be used as a teaching tool to visualize the transition from idealized laminar behavior to real, turbulent dissipation. We did not perform the experiment using oil because, in our configuration, it would have required a large amount of oil, most of which would be wasted, and the corresponding operating time t_f would be too short to be measured with sufficient accuracy. One would practically need access to an oil reservoir and large-diameter pipes to make such an experiment feasible.

4. Conclusions

Our analysis shows that the 'self-flowing flask' configuration cannot sustain motion beyond very short times. Theoretical predictions indicate operating times of only a few seconds for realistic geometries. These values are optimistic upper bounds, since the model deliberately neglects turbulence inside the hose, thus overestimating the actual duration of the flow. Yet, even under these favorable assumptions, the predicted lifetimes are still much shorter than the seemingly steady, almost never-ending circulation displayed in fabricated online videos.

In conclusion, both the theoretical framework and simple experiments, decisively rule out perpetual motion in this setup. Any apparent self-refilling behavior is transient and rapidly suppressed by irreversible energy dissipation. Sustaining the flow would therefore require an external energy input.

Acknowledgments

The author thanks Antonino Cilione for creating nice video simulations of Boyle's self-flowing flasks based on the theoretical model developed in this article. The author gratefully acknowledges Scuola Normale Superiore for supporting the open-access publication of this article.

Conflict of interest statement

The author has no conflicts of interest to disclose.

Data availability statement

All data that support the findings of this study are included within the article (and any supplementary files).

Appendix. Solutions to the Cauchy problem

We summarize here the exact solutions to the Cauchy problem in equation (9). The three cases are distinguished according to the sign of Δ.

1. $\Delta > 0$:

$$v_p(t) = \frac{v_+ - v_- R(t)}{1 - R(t)}, \tag{18}$$

where

$$R(t) \equiv \frac{v_0 - v_+}{v_0 - v_-} \exp\left(\frac{\sqrt{\Delta}}{W} t\right), \qquad v_\pm \equiv \frac{-Y \pm \sqrt{\Delta}}{2X}. \tag{19}$$

The operating time is

$$t_f = \frac{\frac{S}{S_C} h + L}{\sqrt{\Delta}} \ln\left(\frac{v_+}{v_-} \cdot \frac{v_0 - v_-}{v_0 - v_+}\right). \tag{20}$$

This situation arises when viscous effects prevail over gravitational ones—such as for very long and narrow tubes or highly viscous fluids, or in cases involving small height differences $H-h$ or low gravitational acceleration.

2. $\Delta = 0$:

$$v_p(t) = v_* - \frac{W}{\frac{W}{v_0 - v_*} + Xt}, \qquad v_* \equiv -\frac{Y}{2X}, \tag{21}$$

with operating time

$$t_f = \frac{2\left(\frac{S}{S_C}h + L\right)}{\left(\frac{S}{S_C}\right)^2 - 1}\left(\frac{1}{v_*} - \frac{1}{v_0 - v_*}\right). \tag{22}$$

This situation is extremely rare and occurs only when there is a perfect balance between viscous effects and gravity-driven ones.

3. $\Delta < 0$:

$$v_p(t) = \frac{\sqrt{-\Delta}\,\tan\left(\phi_0 + \frac{\sqrt{-\Delta}}{2W}t\right) - Y}{2X}, \tag{23}$$

where

$$\phi_0 \equiv \arctan\left(\frac{2X\,v_0 + Y}{\sqrt{-\Delta}}\right), \tag{24}$$

with operating time

$$t_f = \frac{2\left(\frac{S}{S_C}h + L\right)}{\sqrt{-\Delta}}\left[\arctan\left(\frac{Y}{\sqrt{-\Delta}}\right) - \phi_0 + k\pi\right], \tag{25}$$

where $k \in \mathbb{Z}$ is chosen so that $t_f > 0$ is minimal. This scenario takes place when gravitational effects prevail over viscous ones—for instance, for short and wide tubes, low-viscosity fluids, or when the height difference $H-h$ or the gravitational acceleration is large.

References

[1] Garrett A J M 1990 Perpetual motion—a delicious delirium *Phys. World* **3** 23–7
[2] Gooday G 2024 The monster mechanical delusion: nineteenth-century controversies concerning perpetual motion *J. Phys.: Conf. Ser.* **2877** 012097
[3] Hidayat M N *et al* 2021 A review on how a perpetual motion machine generates electrical power *IOP Conf. Ser.: Mater. Sci. Eng.* **1098** 042063
[4] Williams H 2024 A perpetual motion machine powered by electromagnetism *Phys. Teach.* **62** 4749
[5] See www.youtube.com/watch?v=syCDkFee1go, www.youtube.com/shorts/sNBBL4ByoSo, www.youtube.com/watch?v=QE9wHXigokc and www.youtube.com/watch?v=CJ1Ko8W7iLk as noteworthy examples
[6] McDonough J M 2007 *Introductory Lectures on Turbulence: Physics, Mathematics and Modeling* (Mechanical Engineering Textbook Gallery)
[7] Nelkin M 2000 Turbulence in fluids *Am. J. Phys.* **68** 310318
[8] See, for instance, www.youtube.com/watch?v=6oNFmDzA4tY
[9] Onsager L 1949 Statistical hydrodynamics *Nuovo Cimento* **6** (**Suppl 2**) 279–287
[10] Eyink G and Sreenivasan K R 2006 Onsager and the theory of hydrodynamic turbulence *Rev. Mod. Phys.* **78** 87–135
[11] Eyink G 2024 Onsager's 'ideal turbulence' theory *J. Fluid Mech.* **988**
[12] See https://en.wikipedia.org/wiki/Navier%E2%80%93Stokes_existence_and_smoothness
[13] Tsaousis D 2008 Perpetual motion machine *J. Eng. Sci. Technol. Rev.* **1** 53–7
[14] Cengel Y and Cimbala J 2006 *Fluid Mechanics: Fundamentals and Applications* (McGraw Hill) ch 8
[15] Blasone M *et al* 2015 Discharge time of a cylindrical leaking bucket *Eur. J. Phys.* **36** 035017
[16] Otto J and Mungan C E 2024 Flow of water out of a funnel *Eur. J. Phys.* **45** 055007
[17] Otto J and McDonald K 2018 Torricelli's Law for Large Holes
[18] Mott R L and Untener J A 2015 *Applied Fluid Mechanics* 7th edn (Pearson) ch 10
[19] Fitzpatrick R 2017 *Theoretical Fluid Mechanics* (IOP Publishing) pp 100–1
[20] Batchelor G K 1967 *An Introduction to Fluid Dynamics* (Cambridge University Press) pp 387–91

[21] Alvaro-Berlanga D, Planet R and Fernandez-Nieves A 2024 Torricelli's experiment and conservation of momentum *Am. J. Phys.* **92** 493497
[22] Synolakis C and Badeer H 1989 On combining the Bernoulli and Poiseuille equation—a plea to authors of college physics texts *Am. J. Phys.* **57** 1013–9
[23] Provenzano D B and Stefanini A 2025 Unblowing bubbles: understanding the physics of bubble deflation through a straw *Am. J. Phys.* **93** 797805
[24] Landau L D and Lifshitz E M 2013 *Fluid Mechanics* vol 6 (Pergamon) pp 54–5
[25] Acheson D J 1990 *Elementary Fluid Dynamics* (Clarendon Press) pp 216–7
[26] Saldana M *et al* 2024 The Reynolds number: a journey from its origin to modern applications *Fluids* **9** 1–34
[27] See https://physlets.org/tracker/ for Tracker
[28] Hicks A and Slaton W 2014 Determining the coefficient of discharge for a draining container *Phys. Teach.* **52** 4347
[29] Batchelor G K 1967 *An Introduction to Fluid Dynamics* (Cambridge University Press) p 597